Measuring ion velocity distribution functions through high-aspect ratio holes in inductively coupled plasmas

G. Cunge, Maxime Darnon, J Dubois, P. Bézard, O Mourey, C. Petit-Etienne, L. Vallier, E. Despiau-Pujo, N. Sadeghi

AIP | Applied Physics Letters

Measuring ion velocity distribution functions through high-aspect ratio holes in inductively coupled plasmas

G. Cunge, M. Darnon, J. Dubois, P. Bezard, O. Mourey, C. Petit-Etienne, L. Vallier, E. Despiau-Pujo, and N. Sadeghi

Citation: Applied Physics Letters **108**, 093109 (2016); doi: 10.1063/1.4942892
View online: http://dx.doi.org/10.1063/1.4942892
View Table of Contents: http://scitation.aip.org/content/aip/journal/apl/108/9?ver=pdfcov
Published by the AIP Publishing

Measuring ion velocity distribution functions through high-aspect ratio holes in inductively coupled plasmas

G. Cunge,[a] M. Darnon, J. Dubois, P. Bezard, O. Mourey, C. Petit-Etienne, L. Vallier, E. Despiau-Pujo, and N. Sadeghi
Laboratoire des Technologies de la Microélectronique, CNRS, 17 rue des Martyrs, 38054 Grenoble, France

(Received 26 October 2015; accepted 16 February 2016; published online 3 March 2016)

Several issues associated with plasma etching of high aspect ratio structures originate from the ions' bombardment of the sidewalls of the feature. The off normal angle incident ions are primarily due to their temperature at the sheath edge and possibly to charging effects. We have measured the ion velocity distribution function (IVDF) at the wafer surface in an industrial inductively coupled plasma reactor by using multigrid retarding field analyzers (RFA) in front of which we place 400 μm thick capillary plates with holes of 25, 50, and 100 μm diameters. The RFA then probes IVDF at the exit of the holes with Aspect Ratios (AR) of 16, 8, and 4, respectively. The results show that the ion flux dramatically drops with the increase in AR. By comparing the measured IVDF with an analytical model, we concluded that the ion temperature is 0.27 eV in our plasma conditions. The charging effects are also observed and are shown to significantly reduce the ion energy at the bottom of the feature but only with a "minor" effect on the ion flux and the shape of the IVDF. © *2016 AIP Publishing LLC*. [http://dx.doi.org/10.1063/1.4942892]

Plasma etching of high aspect-ratio (AR) structures is more challenging at each new technological node. Etching profile control is rendered difficult by the ions' bombardment of the sidewalls of the feature because the velocity vector of ions is not always perpendicular to the surface.[1] Furthermore, ion loss on the sidewall reduces the ion flux at the bottom of the feature (which depends on AR) and is thus participating in aspect ratio dependant etching and can lead to etch stop. Several physical phenomena can lead to ions arriving at the wafer/feature's bottom with a significant off-normal angle. First, due to their thermal motion (and associated temperature T_i), ions have a transverse velocity distribution when they enter the sheath. In the high density plasmas at low pressures, the sheaths are collisionless, but the initial ion transverse velocity is conserved (the ion velocity distribution function (IVDF) is a drifting Maxwellian in the sheath), leading to a significant spread in the ion angular distribution.[2,3] It must be underlined that the off normal angle of incidence α of an ion is such that $\tan(\alpha) = v_{th}/V$, where v_{th} is the transverse velocity at the sheath edge and V is the vertical velocity, which depends on the sheath voltage. Therefore, in high density plasmas, the angular distribution of ions impinging on the substrate will depend considerably on the ion energy, i.e., on the dc self-bias voltage of the capacitively coupled rf electrode.

Ion transport inside features can also be significantly impacted by the differential charging effects, which deflect the ions to the sidewalls and reduces their flux and energy at the bottom of the features.[4] In insulators, electrons tend to accumulate on the upper part of the feature due to their isotropic velocity distribution while the positive ions accumulate at the bottom of the feature. The resulting electric field bends the ion trajectories towards the sidewalls of the feature, thus reducing their flux and energy at the bottom of the feature, which can lead to etch stop or twisting[5] of the high AR features. Since the AR of the etch structures is continuously increasing due to the IC miniaturization, understanding ion transport in the high AR structures is important for the development of future processes.

Unfortunately, it is difficult to measure the ion flux and energy *at the bottom* of features during plasma etching. Kurihara and Sekine[6] have used a mass spectrometer embedded in the powered electrode of a magnetron etcher and in front of which they have placed a capillary plate. The MS thus sample ions at the exit of the high AR holes drilled in the capillary plate. They have compared the transmittance of high aspect ratio hole with a simplified analytical model. Since unrealistically high T_i (>0.5 eV) were needed to fit the measured fluxes, it was concluded that the charging effect (not included in the model) was playing a major role in controlling the flux and energy of the transmitted ions.

We have also used capillary plates to analyze ion transport in the high aspect ratio holes. The IVDF are measured at the wafer surface in an industrial inductively coupled plasma (ICP) reactor (from AMAT and designed to etch 300 mm diameter wafers and described elsewhere[7–10]) with a multigrid retarding field ion energy analyzer (RFEA) from IMPEDANS.[11,12] We focus on helium plasmas at 10 mTorr. With 750 W ICP power, the ion flux measured at the radial wall boundary[13] is 1 mA cm^{-2}. At the wafer, this current is about twice higher, which corresponds to a plasma density of about 2.4×10^{10} cm^{-3} and a sheath thickness >1.3 mm for a dc self-bias voltage of 100 V.

The 4 grid RFEA analyzer is fixed on a 300 mm diameter anodized aluminum wafer, as shown in Fig. 1(a). The ions are collected through 800 μm diameter holes drilled in the Al_2O_3 cover, which is protecting the front face of the sensor. Just underneath these holes, the first grid (50 μm Nickel mesh) is electrically connected to the 300 mm wafer and prevents the plasma from entering the analyzer. It also serves as a potential reference: the dc voltage on this

[a]E-mail: gilles.cunge@cea.fr

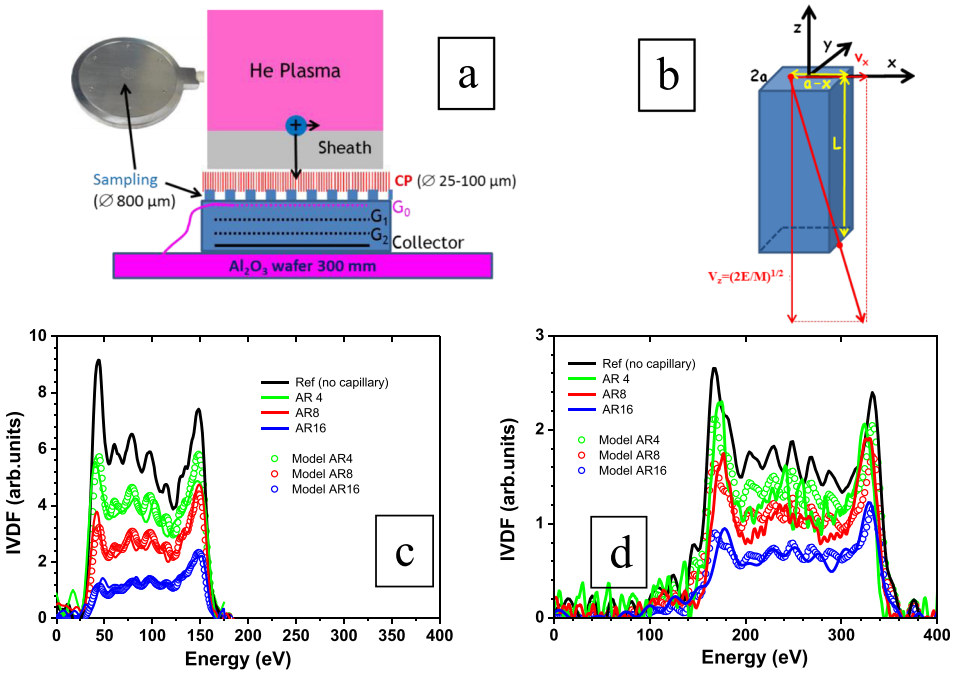

FIG. 1. (a) Schematic of the 4 grid RFEA sensor on the 300 mm diameter wafer. The capillary plate (CP) is lying on the Al_2O_3 cover of the sensor. (b) A square shape hole, which is used to model the cylindrical holes of radius R of real CP, has an aspect ratio of L/2a, where 2a is the square side dimension. The ion vertical velocity is related to their energy E. In this example, the ion transverse velocity v_x is the maximum possible allowing it to pass through the hole. (c) and (d) IVDF measured without capillary plate (black curve) and with CP4, CP8, and CP16 (plain lines). He plasma at 10 mTorr with (c) 750 W ICP power and 200 W rf bias power and (d) 400 W ICP power and 300 W rf bias power. Open symbols are obtained from Eq. (4) with the Reference IVDF as an input and assuming $T_i = 0.27$ eV.

electrode is the same as the dc self-bias voltage of the 300 mm wafer. The second grid is polarized positively to repel electrons. The voltage of the third grid can be swept to discriminate ions as function of their energy: by recording the corresponding current on the fourth plate, one gets an I(V) curve whose derivative directly provides the IVDF. All grids float at the wafer potential.[12]

The capillary plates (from Hamamatsu) are stuck by kapton™ tape in front of the RFA, as shown in Fig. 1(a). They consist of 2 cm diameter, 0.4 mm thick glass substrates drilled with cylindrical holes and with an open area of about 55%. We used capillary plates with holes of 25, 50, and 100 μm diameters. Therefore, the RFA probes IVDF at the exit of the holes with AR of 16, 8, and 4, respectively, which hereafter will be referred by CP4, CP8, and CP16, respectively. We underline that the capillary plate (CP) holes' diameter is at least 13 times smaller than the estimated sheath thickness. Therefore, there is negligible distortion of the sheath, which remains flat above the CP (i.e., sheath bending is not responsible for an additional angular dispersion). Furthermore, the 0.4 mm thick CPs form a capacitance in series with the sheath capacitance. As a result, the real dc self-bias voltage at the CP surface is smaller than the real one on the wafer. However, since the CP is thin while its dielectric constant is high (about 6), this effect is negligible (calculated 5% difference[14]).

Figs. 1(c) and 1(d) show the IVDF for two different plasma conditions (self-bias voltages of −100 V and −250 V). Without capillary plate, the IVDF exhibit the typical saddle shape structure observed in RF discharge containing low mass ions.[15] The two predominant peaks correspond to light He^+ ions. The complex shape in between these peaks is attributed to parasitic heavier species, including Al^+ ions.

Figs. 1(c) and 1(d) show that ion transport depends strongly on the AR of the holes: the ion flux (integral of the IVDF) dramatically drops when the AR is increased. Furthermore, the attenuation depends on the energy with a much higher attenuation at a lower energy. Indeed, the typical "saddle" structure of the unperturbed IVDF is distorted after passing through the capillary plates. As expected, the flux of low energy ions is much more damped than the flux of higher energy ions because the ion angular distribution becomes broader when the ion energy is reduced, leading to an enhanced loss of ion in the high AR holes.

We underline that our DC potential reference V_{ref} is measured on the first grid of the analyzer *underneath* the capillary plate (Fig. 1(a)). It means that under our conditions, charging effects will impact the ion flux but not the measured ion energy: the ions will always pass through the first grid of the analyzer (underneath the CP) with an energy given by V_p-V_{ref}, and even if charging slows down the ions while they pass through the CP, this will not be apparent. However, the ion flux will be reduced due to ion deflection and loss (neutralization) on the sidewalls. To determine if the reduction of the ion flux that is observed when the hole's AR is increased (Figs. 1(c) and 1(d)) is due to the ion angular distribution or to the charging effects, it is necessary to model ion transport in holes.[6]

Let us consider the case of a square shaped hole, as shown in Fig. 1(b). This particular shape allowed to find an analytical solution for the transmittance of the hole by using Cartesian coordinates and the difference with a cylinder of same surface is expected to be negligible. The sides of the square are $2a$, with $a = \sqrt{\pi/4}.R$, where R is the radius of the cylindrical hole of same area. The cylinder length is L, and thus, the hole's AR = L/2a. For the incoming ions, we consider the velocity $V_z = \sqrt{2E/m}$ along the hole axis (where E is the ion energy given by the sheath voltage) and an isotropic Maxwellian velocity distributions on the x and y directions

$$\varnothing(v_i) = \sqrt{\beta/\pi} e^{-(\beta v_i^2)}, \quad (1)$$

where v_i states, for either v_x or v_y, the ion off normal velocity components, and $\beta^2 = m/(2kT_i)$. The situation being similar

along the x and y directions, the transmission factor P of the hole (ratio of the ion flux which exit the hole divided by the incoming flux) is

$$\sqrt{P} = \left(\frac{\beta}{[\sqrt{\pi}2a]}\right) \int e^{-(\beta v_i)^2} dv_i \int dx. \quad (2)$$

The integration limits are calculated geometrically from Fig. 1(b). Let us consider the situation for $v_i > 0$. The upper integration limit for v_i is $v_u = (\frac{2aV}{L})$, and for a fixed v_i, the upper integration limit in x is $x_u = a - (\frac{Lv_i}{V})$. Since the same conclusion applies for $v_i < 0$, a factor 2 is introduced, leading to

$$\sqrt{P} = \left(\frac{2.\beta}{[\sqrt{\pi}2a]}\right) \int_0^{v_u} e^{-(\beta v_i)^2} dv_i \int_{-a}^{x_u} dx, \quad (3)$$

whose analytical solution is

$$P = \frac{1}{\pi}\left[\sqrt{\pi}\,\mathrm{erf}\left(0, \frac{V\beta}{AR}\right) - \frac{AR}{V\beta}\left(1 - e^{-\left(\frac{V\beta}{AR}\right)^2}\right)\right]^2, \quad (4)$$

where erf is the error function: $\mathrm{erf}(0,b) = \frac{2}{\sqrt{\pi}} \int_0^b e^{-t^2} dt$. Eq. (4) allows one to calculate the attenuation of the ion flux as a function of the hole's AR and of the ion energy E and their temperature T_i at the sheath edge. Given a reference IVDF $f_v(E)$ (i.e., measured without the capillary plate), Eq. (4) can be used directly to predict how the shape of this reference IVDF should evolve after passing through the holes of a given AR with only one adjustable parameter: the ion temperature T_i at the sheath edge.

Fig. 1(c) shows the IVDF measured without capillary plate and with CP4, CP8, and CP16. The open symbols are obtained from Eq. (4) with $T_i = 0.27$ eV and using the reference IVDF without capillary plate as an input $f_v(E)$. Fig. 1 shows that Eq. (4) allows to capture remarkably well the variation of the IVDF's shape as a function of the hole AR. The agreement is indeed so good that we can get a precise estimation of the ion temperature at the sheath edge with this technique. Fig. 2 shows the IVDF measured through CP16, together with the prediction from Eq. (4) for three different ion temperatures (0.15, 0.27, and 0.45 eV). The result of the model is indeed quite sensitive to T_i, and the ion temperature is 0.27 ± 0.03 eV. The accuracy on determining T_i is even better when we fit the variations of the total ion flux as a function of AR, as shown on the inset of Fig. 2, because this flux is obtained by integration of the IVDF and less sensible to noise. The measured $T_i = 0.27$ eV is far above the expected neutral temperature (<0.07 eV near the wafer[16]), but it is in excellent agreement with ion temperatures measured in the high density plasma.[17] From a long set of experiments in various gases and rf power (not shown), we concluded that ions in ICP reactor operated in typical conditions have a temperature of about 2500–3000 K.

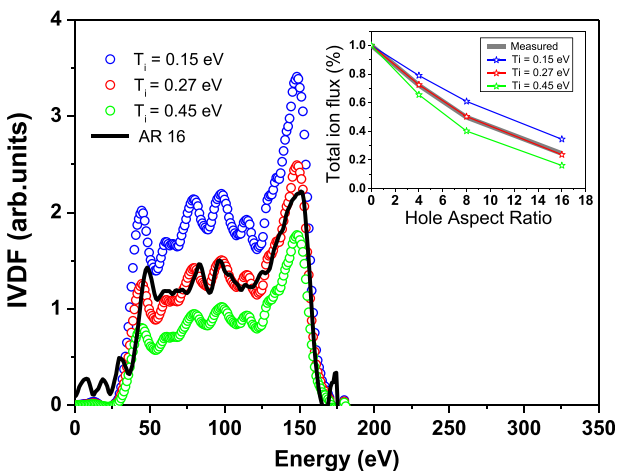

FIG. 2. IVDF measured through CP16 (black) and fit from Eq. (4) using three different T_i (0.15, 0.27, and 0.45 eV). The inset shows the variations of the total ion flux as a function of AR together with the result of Eq. (4) for the same three T_i.

All our experimental data set can be explained by assuming that the angular velocity distribution of ions is solely responsible for the attenuation of their flux as they pass through high aspect holes. In other words, it is most likely that charging effects are negligible under our conditions. This conclusion is opposite to that of Kurihara and Sekine. The main reason for this discrepancy is the model they have used for the calculation of the ion flux's attenuation as a function of the hole's AR, which was excessively simplified and did not account for the uniform density distribution of ions over the entire entering surface of the hole. This was leading to a large overestimation of the value of T_i needed to explain their measurements.

Nevertheless, our conclusions remain surprising since we are using glass plates, which are good insulator materials. However, a significant difference remains between a capillary plate and a real feature: the latter has a bottom which charges positively, therefore increasing the repulsing potential compared to an open cylinder. This situation is somewhat similar to the difference between etching of a conductive or an insulator material: in the former case, only the mask (insulator) can charge and the voltage in the hole does not exceed a few volts,[18] while in the latter case, positive charge accumulation at the bottom of the feature can easily lead to a repulsive potential of 60 V.[19] Observing the strong charging effects thus requires a bottom of the feature to accumulate positive charges. To get further insight into the charging effects, we have superposed a CP4 on top of a CP8 capillary plate, as shown in Fig. 3. As a result, the AR = 4 cylinders now have a bottom with a 45% closed area and should be subjected to additional charging compared to an open CP4 capillary. In Figs. 3(a) and 3(b), we show the IVDF measured through the stacked CP. Fig. 3 also shows the IVDF that one would expect (Eq. (4)) at the exit of a hole of AR = 8 by assuming that the reference incoming IVDF is the one measured through CP4 (Fig. 1(c)). In other words, we used Eq. (4) to predict how the IVDF measured at the exit of CP4 should be modified when passing through the holes of CP8. Since we do not consider charging effects in Eq. (4), a good agreement between the CP4 + CP8 stack and the model would indicate that charging is negligible.

However, Fig. 3(b) shows that there are significant discrepancies between the measured IVDF and the model in this case. In particular, the measured IVDF in Fig. 3(b) is clearly "cut" below 50 eV, although ions with energy down to 30 eV should be able to pass through the AR8 hole without charging. The overall ion flux is also significantly smaller

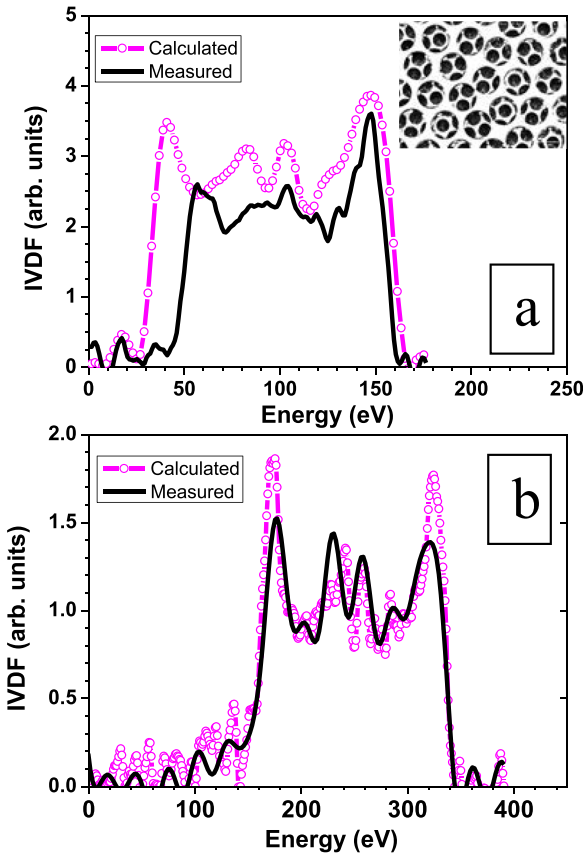

FIG. 3. (a) and (b) The IVDF measured for plasma conditions of Fig. 1(c) and 1(d), respectively, after passing through the stack CPs (black). The magenta symbols are obtained by using Eq. (4) to predict how the incoming IVDF (measured through CP4) should evolve after passing through a CP8. Inset: top view optical image of the CP4 + CP8 stack.

than the expected. This is attributed to a positive charge accumulation at the bottom of the CP4 hole, leading to a potential barrier of about 50 V that the ions must overcome to pass through the holes. As a consequence, we expect that the "real" IVDF should be shifted towards lower energies by about 50 eV (reminding that we cannot capture this energy shift with our set up (Fig. 1(a)). However, it remains difficult to analyze in detail the impact of the charging effects on the IVDF shapes because charging does not lead to flat equipotential surfaces on the sidewalls of the hole and could result in focusing/defocusing effect that are difficult to model. Yet, in good agreement with the hypothesis above, Fig. 3(c) shows that when the rf-bias power is increased to such an extent that the energy of all ions is far above the hole charging potential, then there is good agreement between calculation and measurements, demonstrating that the impact of charging on the ion flux becomes negligible in this case. More precisely, the main effect of charging at high energy is to induce a shift of about 50 V in the IVDF.

Therefore, our results show that in an He plasma, the charging effects do not have significant impact on the flux of ions that reach the bottom of features with AR < 16. This transmitted flux is likely determined by the ion angular distribution, which is broad due to a relatively high T_i at the sheath edge. However, charging results in a decrease of the ion energy, which is much more pronounced in the presence of a feature's bottom that can charge positively. Similar conclusions are obtained in Ar and CF_4 plasma (not shown), in which the ion mass is much larger.

This work was partly supported by the French RENATECH Network.

[1]R. A. Gottscho, C. W. Jurgensen, and D. J. Vitkavage, J. Vac. Sci. Technol. B **10**(5), 2133 (1992).
[2]J. R. Woodworth, M. E. Riley, P. A. Miller, G. A. Hebner, and T. W. Hamilton, J. Appl. Phys. **81**(9), 5950–5959 (1997).
[3]N. Mizutani and T. Hayashi, J. Vac. Sci. Technol. A **19**(4), 1298–1303 (2001).
[4]G. S. Hwang and K. P. Giapis, J. Appl. Phys. **82**(2), 566–571 (1997).
[5]M. Wang and M. J. Kushner, J. Appl. Phys. **107**, 023309 (2010).
[6]K. Kurihara and M. Sekine, Plasma Sources Sci. Technol. **5**, 121–125 (1996).
[7]C. Petit-Etienne, E. Pargon, S. David, M. Darnon, L. Vallier, O. Joubert, and S. Banna, J. Vac. Sci. Technol. B **30**(4), 040604 (2012).
[8]M. Darnon, G. Cunge, and N. S. J. Braithwaite, Plasma Sources Sci. Technol. **23**(2), 025002 (2014).
[9]G. Cunge, M. Fouchier, M. Brihoum, P. Bodart, M. Touzeau, and N. Sadeghi, J. Phys. D: Appl. Phys. **44**(12), 122001 (2011).
[10]G. Cunge, P. Bodart, M. Brihoum, F. Boulard, T. Chevolleau, and N. Sadeghi, Plasma Sources Sci. Technol. **21**(2), 024006 (2012).
[11]M. Brihoum, G. Cunge, M. Darnon, D. Gahan, O. Joubert, and N. S. J. Braithwaite, J. Vac. Sci. Technol. A **31**(2), 020604 (2013).
[12]D. Gahan, S. Daniels, C. Hayden, P. Scullin, D. O'Sullivan, Y. T. Pei, and M. B. Hopkins, Plasma Sources Sci. Technol. **21**(2), 024004 (2012).
[13]N. S. J. Braithwaite, J. P. Booth, and G. Cunge, Plasma Sources Sci. Technol. **5**, 677 (1996).
[14]O. Joubert, G. Cunge, B. Pelissier, L. Vallier, M. Kogelschatz, and E. Pargon, J. Vac. Sci. Technol. A **22**, 553 (2004).
[15]M. A. Lieberman and A. J. Lichtenberg, *Principle of Plasma Discharges and Material Processing* (J. Wiley, New York, 1994), ISBN: 978-0-471-72001-0.
[16]G. Cunge, R. Ramos, D. Vempaire, M. Touzeau, M. Neijbauer, and N. Sadeghi, J. Vac. Sci. Technol. A **27**(3), 471 (2009).
[17]N. Sadeghi, M. vanDeGrift, D. Vender, G. M. W. Kroesen, and F. J. deHoog, Appl. Phys. Lett. **70**(7), 835–837 (1997).
[18]K. P. Giapis and G. S. Hwang, Thin Solid Films **374**(2), 175–180 (2000).
[19]G. S. Hwang and K. P. Giapis, J. Appl. Phys. **82**(2), 572–577 (1997).